CTuK5 **1:00 pm**

Waveguide Electro-optic Modulators Based on Organic Self-assembled Superlattices (SAS)

Zhifu Liu, S.T. Ho, and S.S. Chang, Department of Electrical and Computer Engineering, Northwestern University, Evanston, Illinois 60208, Email: zhifuliu@mailexcite.com

T.J. Marks, Department of Chemistry and Materials Research Center, Northwestern University, Evanston, Illinois 60208

Organic materials have attracted remarkable interest recently as promising candidates for electro-optic (EO) devices because of their substantially low dispersion of EO coefficients compared to conventional inorganic EO materials such as $LiNbO_3$.[1,2] Organic materials with EO coefficients higher than r_{33} of $LiNbO_3$ have been reported.[3,4] Recently a method of fabricating self-assemble superlattice (SAS) layers of polymer materials has been discussed.[5] The SAS layers were intrinsically accentric, and second harmonic generation (SHG) and EO effects have been demonstrated without external electric field poling process.[6,7]

A prototype symmetric waveguide EO modulator was proposed. Fig. 1 shows the cross section of the waveguide structure of the EO modulator based on GaAs substrate. A 0.5 μm gold layer (the lower electrode) was deposited on the GaAs substrate. Then a SiO_2 layer was fabricated by PECVD method. The EO SAS layers were grown on a BCB (Cyclotene 3022-35) layer, and then were covered by another BCB layer. The two BCB layers functioned as two guiding layers and made the waveguide symmetric. While the thickness of the EO active SAS layer was less than 1.496 μm at a wavelength of 1.064 μm, this symmetric waveguide remains a single mode waveguide.[8]

A 2.5 μm Cytop (a fluorinated polyether) layer was spin-coated on the upper BCB layer to reduce the contact loss of the wave energy. Finally, another gold layer (the upper electrode) was deposited on the Cytop layer.

The RF bandwidth is related to the velocity mismatch between optical and RF waves and the RF electrode loss. For low loss materials, parameters $n_{eff\text{-}opt}$ and $n_{eff\text{-}rf}$ are needed for the evaluation of the RF bandwidth. Index $n_{eff\text{-}opt}$ was estimated using a multi-layer waveguide configuration. Index $n_{eff\text{-}rf}$ was given by

$$n_{eff\text{-}rf} = \sqrt{\frac{C}{C_0}},$$

where C was the capacitance with materials presented and C_0 was that without materials (replaced by air) for a unit long segment of the waveguide. The capacitance calculation was made using finite element analysis methods. The characteristic impedance Z linked with the capacitances by

$$Z = \frac{1}{c\sqrt{CC_0}},$$

where c is the speed of light in vacuum.

The effective optic refractive index $n_{eff\text{-}opt}$ is 1.556 at a wavelength of 1.064 μm. The capacitance of the sample C is 106 pF. While the materials are replaced by air, the capacitance C_0 of the virtual sample is 37.8 pF. The effective RF refractive index $n_{eff\text{-}rf}$ is 1.675. The characteristic impedance Z is 52.7 Ω, which is quite close to the 50 Ω ideal value. The difference between the $n_{eff\text{-}opt}$ and $n_{eff\text{-}rf}$ is about 0.119, and this makes sure that one can achieve a bandwidth of 40 GHz for an EO

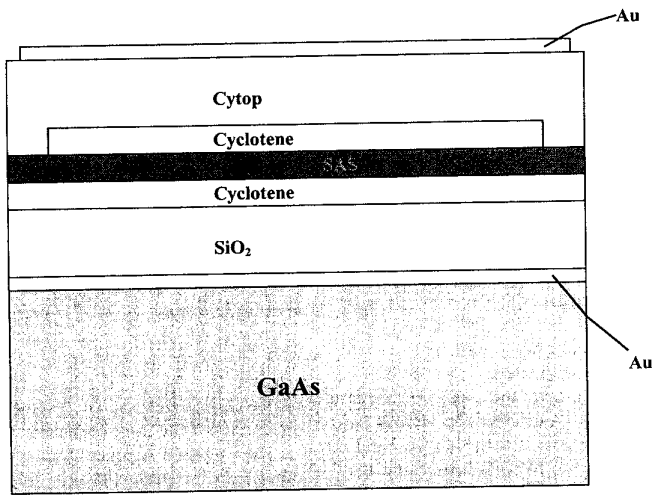

(a)

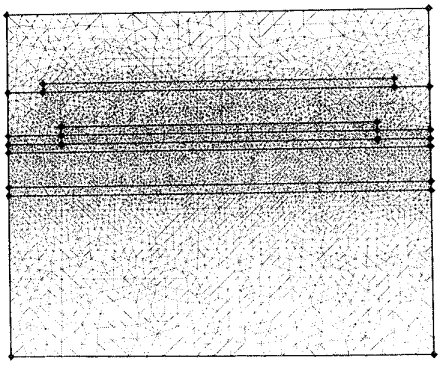

(b)

CTuK5 Fig. 1. The cross section of the waveguide EO modulator. (a) The geometry of the EO modulator, and (b) the node divisions for finite element analysis.

(a)

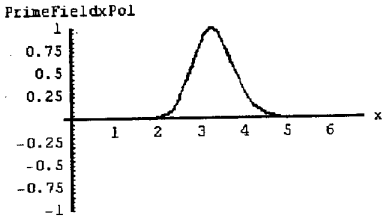

CTuK5 Fig. 2. (a) The refractive index profile, and (b) the electric field distribution (near the central part of the waveguide) along the vertical direction.

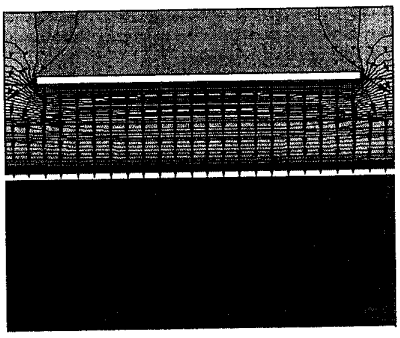

CTuK5 Fig. 3. The external electric field and potential distributions of the EO modulator.

modulator up to 3 cm long. While the applied voltage between the two electrodes is 100 V, the voltage difference between the upper and lower surfaces of the EO active SAS layer (0.5 μm thick) is about 4.15 V. For a 1 cm long EO modulator with 5 V driving voltage, the equivalent driving voltage for a longitudinal EO modulation configuration is about 4.2 kV.

References

1. J. Badan, R. Hierle, A. Perigaund, and J. Zyss, ACS Symp. Ser. **233**, 81–107 (1983).
2. A.M. Prokhorov and Yu. S. Kuz'minov, *Physics and chemistry of crystalline lithium niobate* (IOP publishing Ltd., Adam Hilger, 1990), pp. 222–223.
3. Y. Shuto, M. Amano, and T. Kaino, IEEE Trans. Photon. Techn. Lett. **3**, 1003 (1991).
4. S.R. Marder, J.W. Perry, and C.P. Yakymyshyn, Chem. Mater. **6**, 1137–1147 (1994).
5. S. Yitzchaik, and T.J. Marks, Acc. Chem. Res. **29**, 197–202 (1996).
6. M.E. Van der Boom, A.G. Richter, J.E. Malinsky, P.A. Lee, N.R. Armstrong, P. Dutta, and T.J. Marks, Chem. Mater. **13**, 15–17 (2001).
7. Y.G. Zhao, A. Wu, H.L. Lu, S. Chang, W.K. Lu, and S.T. Ho, Appl. Phys. Lett. **79**(5), 587–589 (2001).
8. R.G. Hunsperger, *Integrated Optics: Theory and Technology* (Springer, Berlin, Germany, 1995), Chapters 2 & 3.

CTuK6 **1:00 pm**

Functionality of Optical Field Transformation in Irregular Waveguide Structures

M. Yang and K.J. Webb, School of Electrical and Computer Engineering, Purdue University, 1285, Electrical Engineering Building, West Lafayette, Indiana 47907-1285, Email: webb@ecn.purdue.edu

Periodic optical elements such as photonic bandgap structures[1] have been widely explored. While these structures perform effectively in some applications, the limited degrees of freedom can dictate their size. We adopt the concept of irregular structures,[2] which have been shown to provide better performance and functionality than periodic structures, with significantly reduced size. We demonstrate both optical mode converter and mode-selective optical cavity structures that can be fabricated using standard semiconductor processing techniques. Frequency-dependent mode conversion illustrates the prospect for wavelength division multiplexing elements and laser cavity mode control. The mode converter function can lead to optimal power splitters.

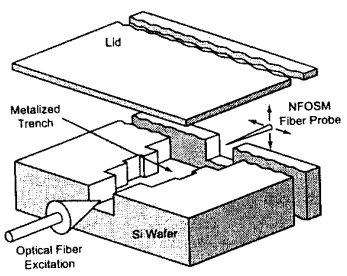

CTuK6 Fig. 1. Schematic diagram of a waveguide with an irregular scattering surface.

The general concept of our irregular waveguide structure is depicted in Figure 1, where the variable width sections provide for field transformation. We treated the discrete waveguide widths as optimization variables in a cost function involving the input field and the desired output field. A multi-resolution strategy was used to arrive at particular designs, where solutions with coarse steps in waveguide width with a small number of sections were refined to smaller steps in width and a larger number of sections during the iterative process. The forward solution, for a particular geometry, was represented by a generalized scattering matrix,[3] where the fields in each uniform section of waveguide were expanded using propagating modes and an adequate number of evanescent modes for convergence. We found that more than one solution can exist, i.e., that there may not be a unique solution.

A TE_{10}/TE_{30} mode converter example operating at 1.55 μm is shown in Figure 2. Figure 2(a) shows the conducting waveguide sidewall geometry, and Figure 2(b) the frequency response for each propagating mode. Complete field transformation is achieved in a length of less than 6.5 wavelengths, with no reflection. This mode converter is a one-to-three power splitter, with an appropriately arranged output waveguide configuration. As a second example, consider the mode selective structure of Figure 3. The reflectivity for the TE_{10} mode at 1.55 μm is 99.8%, while the TE_{20} mode has very low reflectivity (0.01%). Therefore, such a structure could act as a cavity mirror to select one mode for lasing at 1.55 μm, in this case.

We have demonstrated the functionality

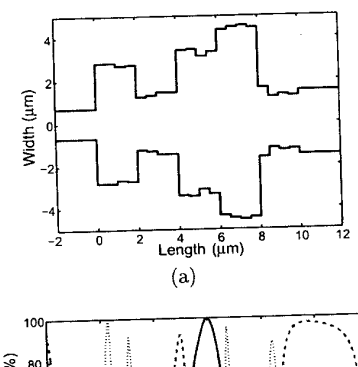

CTuK6 Fig. 2. (a) 1.55 μm TE_{10}/TE_{30} mode converter, and (b) frequency response of the propagating mode. Solid: transmitted TE_{30}; dashed: transmitted TE_{10}; dotted: reflected TE_{10}.

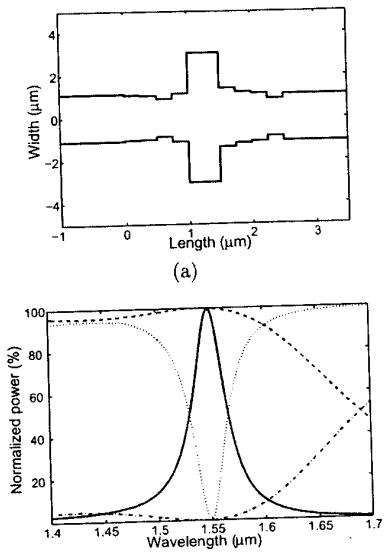

CTuK6 Fig. 3. (a) 1.55 μm TE_{10}/TE_{20} mode-selective structure, and (b) frequency response of the propagating mode. Solid: reflected TE_{10}; dashed: transmitted TE_{20}; dotted: transmitted TE_{10}; and dot-dashed: reflected TE_{20}.

achievable with optimized, irregular optical field transformation components. The compact design geometries we have obtained are within the resolution limits of electron beam lithography, and could be fabricated on a semiconductor wafer with current technology.

References

1. E. Yablonovitch, "Photonic band-gap structures," J. Opt. Soc. Am. B **10**, 283–295 (1993).
2. T. Haq, K.J. Webb, and N.C. Gallagher, "Optimized Irregular Structures for Spatial- and Temporal-Field Transformation," IEEE Trans. Microwave Theory Tech. **46**, 1856–1867 (1998).
3. T.S. Chu and T. Itoh, "Generalized scattering matrix method for analysis of cascaded and offset microstrip step discontinuities," IEEE Trans. Microwave Theory Tech. **34**, 280–284 (1986).

CTuK7 **1:00 pm**

Range Correlator Demonstrated in 0.5 GHz Spectral Holographic Gratings at 1.5 Microns

Z. Cole, K.M. Rupavatharam and K.D. Merkel, Spectrum Lab, Montana State University, Bozeman, MT 59717, Email: cole@spectrum.montana.edu

T. Böttger, W.R. Babbitt and R.L. Cone, Department of Physics, Montana State University, Bozeman, MT 59717

Spectral-spatial holographic (SSH) materials are ideal for performing a variety of high bandwidth analog correlations because of potential band-